Nematic kink states in a laser field

S. K. Srivatsa* and G. S. Ranganath†
Raman Research Institute, Bangalore 560 080, India
(Received 1 February 1999)

We have investigated the nonlinear optical interaction of uniform and kink states of a nematic and a ferrofluid-doped nematic (ferronematic) liquid crystal with an incident laser field. We find that the transition between the permitted uniform oreintational states of these systems is of first order in the case of nematics, and of second order in the case of ferronematics. In the latter case we also find the phenomenon of reentrance. We find new kink states in a magnetic field with topological winding different from π in the case of nematics, and 2π in the case of ferronematics. In ferronematics, due to grain segregation the phase diagrams for uniform and kink states are entirely different. In these systems we find a first or second order structural transformation from a single kink into a pair of kinks. Further, we obtain a rich variety of kink states as the intensity of the laser field is varied. [S1063-651X(99)12811-3]

PACS number(s): 61.30.Gd, 61.30.Jf, 42.70.Df

I. INTRODUCTION

Nonlinear optical effects in liquid crystals have received a great deal of attention in recent times [1,2]. The light induced Fréederickz transition, director reorientation, and grating effects have been extensively studied [3,4] both theoretically and experimentally. However, optical effects that can occur when a laser is used for probing topological defects appear to have not attracted as much attention. Here we address ourselves to nonlinear optical effects on nonsingular topological defects called planar walls. In these the director distortions are in one dimension and are often called solitons in literature [5]. Yet, unlike true solitons these do not preserve their shape and velocity after a pairwise collision. Further, since these are like kinks structurally, we refer to them as kinks hereafter.

Kink states in liquid crystals were first discussed by Helfrich [6]. These are static walls in a nematic in the presence of an external static magnetic field. Walls arise because of the degeneracy in the director orientation, which can be either parallel or antiparallel to the external field. There can be pure twist walls or splay-rich or bend-rich walls. In each case the director turns through 180° along a direction normal to the wall. Also, there can be kinks known as Brochard-Leger walls which are associated with the Freederickz transition. These arise from the degeneracy in director tilt with respect to the field above a threshold value. Kinks also appear naturally in the form of a lattice [7,8] near a field induced transition of a cholesteric to a nematic state. It has been suggested [9] that kinks also play an important role in a smectic C^* to smectic A transition.

The electric field associated with a laser beam can simulate the effect of an external static field, since the torque on the nematic director depends quadratically on the field. The coupling between the director and the electric field of the laser beam arises due to optical dielectric anisotropy. However, this is possible only if the intensity is high enough. With the availability of the high power lasers nonlinear effects have become relevant. In such cases it is necessary to solve self-consistently both equations of elastic equilibrium and Maxwell's equations of electrodynamics.

We have worked out the structural transitions between different permitted kinks in the presence of a laser field and a static magnetic field. For a certain range of parameters, we find a new kink state which connects the director along the electric field to one perpendicular to it. Such a kink state is forbidden in static fields in view of the inherent symmetry of the nematics. We have extended our studies to ferronematic liquid crystals. Here also we obtain many new kink states, and the phase diagram of structural transformations in kink states exhibits tricritical points and reentrant phenomenon.

II. THEORY

The free energy density of a nematic has contributions from both the elastic deformations and externally applied fields. In the one elastic constant approximation and with a static magnetic field it is given by [10]

$$\mathcal{F}_n=\frac{K}{2}[(\boldsymbol{\nabla}\cdot\mathbf{n})^2+(\boldsymbol{\nabla}\times\mathbf{n})^2]-\frac{\chi_\perp}{2}\mathbf{H}^2-\frac{\chi_a}{2}(\mathbf{n}\cdot\mathbf{H})^2, \quad (1)$$

where $\mathbf{n}$ is the nematic director, K is the Frank elastic constant, $\mathbf{H}$ is the static magnetic field, and χ_a is the diamagnetic anisotropy which is equal to $(\chi_\parallel-\chi_\perp)$, with $\chi_\parallel$ and $\chi_\perp$ as the diamagnetic susceptibilities parallel and perpendicular to the director, respectively. In a free sample, $\mathbf{n}$ will be either parallel or perpendicular to the magnetic field depending on whether χ_a is positive or negative.

Ferronematics are a dilute uniform suspension of needlelike magnetic grains in a nematic. The grains are preferentially aligned along the local nematic director when the system is cooled from its isotropic phase. The director orientation in these systems may be altered by the application of static magnetic fields as low as 10–100 G. On the other hand, to effect the same change in a normal nematic, magnetic fields as high as 1 kG would be required because of the small value of the diamagnetic anisotropy. Further, if the

*Electronic address: vatsa@rri.ernet.in
†Electronic address: gsr@rri.ernet.in

grain concentration is low enough we can ignore the effects of magnetic grains on the passage of a light wave through the medium. In this case there are additional contributions to the free energy density, one due to ferromagnetic interaction with the external field and the other due to entropy of mixing between the guest (magnetic grains) and host (nematic). The net contribution is given by [11]

$$\mathcal{F}_{fn} = -\mathbf{M}\cdot\mathbf{H} + \frac{f k_B T \ln f}{v}. \tag{2}$$

Here f is the volume fraction of ferromagnetic grains in the nematic matrix, $\mathbf{M}$ is the magnetization in the medium, k_B is Boltzmann's constant, T is the absolute temperature, and v is volume of the sample. Due to mechanical coupling between the grains and the director $\mathbf{n}$, the average magnetization $\mathbf{M}$ is along $\mathbf{n}$, and the magnitude of $\mathbf{M}$ is f times the average grain magnetization. In these systems the uniform state has a constant f. However, as large director distortions are associated with the kink state, f varies substantially from point to point in a kink, resulting in ''grain segregation.'' This is due to migration of ferromagnetic grains from energetically less favorable regions into energetically more favorable regions.

Now we consider the contribution to the free energy density by electric and magnetic fields of a laser beam. Even though these fields oscillate at a high frequency of 10^{14}–10^{15} Hz, they can exert a torque on $\mathbf{n}$ since the torque arising from dielectric and diamagnetic anisotropy of the medium depends quadratically on the field. In principle, there is a contribution to the free energy density from both electric and magnetic fields. In fact, the two energy densities are equal in vacuum. But, in nematics both the diamagnetic susceptibility and its anisotropy are very small each being of the order of 10^{-6}. Hence for optical fields $\epsilon|\mathcal{E}|^2 = |\mathcal{H}|^2$, where ϵ is the dielectric constant, $\mathcal{E}$ and $\mathcal{H}$ are electric and magnetic fields of the laser beam. In an anisotropic medium the free energy density due to the optical field is given by [3,12]

$$\mathcal{F}_o = -\sum_{j,k} \frac{\epsilon_{jk}}{8\pi}\mathcal{E}_j(\mathbf{r},t)\mathcal{E}_k(\mathbf{r},t), \quad j,k = x,y,z, \tag{3}$$

where, ϵ_{jk} is the second rank dielectric tensor of the medium, and $\mathcal{E}_j(\mathbf{r},t)$ is a component of the electric field of the light wave. The equations of elastic equilibrium is obtained by minimizing the total free energy $\mathcal{F} = \int(\mathcal{F}_n + \mathcal{F}_{fn} + \mathcal{F}_o)dV$. In the present case, in addition to these equations, we have to solve the Maxwell's wave equation for the laser wave in the medium. That is, $\mathcal{E}$ must be obtained from

$$\nabla\times[\nabla\times\mathcal{E}(\mathbf{r})] - \frac{\omega^2}{c^2}\mathcal{D}(\mathbf{r}) = \mathbf{0}. \tag{4}$$

ω is the frequency of the light wave, c is the velocity of light, and $\mathcal{D}$ is the displacement vector whose components are given by $\mathcal{D}_j = \Sigma_k \epsilon_{jk}\mathcal{E}_k$. The determination of the steady state structure requires a knowledge of $\mathcal{E}$ permitted by the Maxwell's equations. Since a nematic is cylindrically symmetric about $\mathbf{n}$, it is optically uniaxial. Then the eigenstates of the electric field vector $\mathcal{E}$, which go through the medium unaltered, are $\mathcal{E}$ parallel and perpendicular to the director $\mathbf{n}$. In this paper, we consider only a splay-rich or bend-rich kink state with its director confined to the x-z plane and having $\mathbf{n}$ varying along z. Also we restrict ourselves to a linearly polarized light wave propagating along the z axis with its electric vector $\mathcal{E}$ along the x axis. Then field $\mathcal{E}$ variations are also along z. The geometry is depicted in Fig. 1(a). It is easy to see from the geometry that the polarization of the light wave is preserved during its passage through the kink. The Maxwell's wave equation is solved in the approximation that the director distortions in the medium are on a length scale large compared to the wavelength of light. Then solutions to the wave equation (4) become [3]

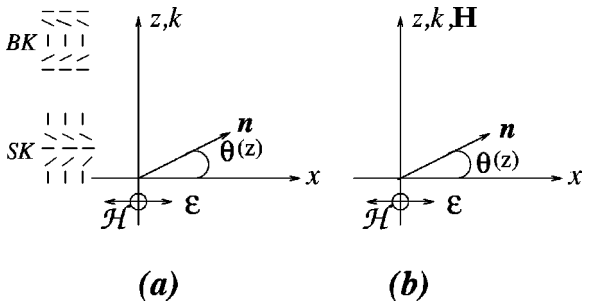

FIG. 1. Geometries showing the orientation of the director $\mathbf{n}$ with respect to the electric field $\mathcal{E}$ of the incident light and a static magnetic field $\mathbf{H}$. (a) $\mathbf{H}=0$, (b) $\mathbf{H}$ is perpendicular to $\mathcal{E}$, $\mathbf{k}$ is the direction of propagation of the light, and $\mathcal{H}$ is the magnetic vector associated with the light which is perpendicular to the plane of the figure. Structures *SK* and *BK* are splay-rich and bend-rich kinks, respectively.

$$\mathcal{E}_x(z) = A(\epsilon_\perp + \epsilon_a \sin^2\theta)^{1/4} \times \exp\left[-ik_0(\epsilon_\parallel\epsilon_\perp)^{1/2}\int^z(\epsilon_\perp + \epsilon_a\sin^2\theta)^{-1/2}dz'\right], \tag{5}$$

$$\mathcal{E}_z(z) = -A\frac{\epsilon_a \sin\theta\cos\theta}{(\epsilon_\perp + \epsilon_a\sin^2\theta)^{3/4}} \times \exp\left[-ik_0(\epsilon_\parallel\epsilon_\perp)^{1/2}\int^z(\epsilon_\perp + \epsilon_a\sin^2\theta)^{-1/2}dz'\right], \tag{6}$$

TABLE I. The various stable and metastable states of the uniform and kink states in the different regions of the phase diagram shown in Fig. 2(a).

Region	Uniform state			Kink state	
	Stable states		Metastable states	Topological charge	Split occurs at
A	$-\pi/2$	$\pi/2$		π	
B	$-\pi/2$	$\pi/2$	0	π	0
C	$\pi/2$	0		$\pi/2$	
D	0	π	$\pi/2$	π	$\pi/2$
E	0	π		π	

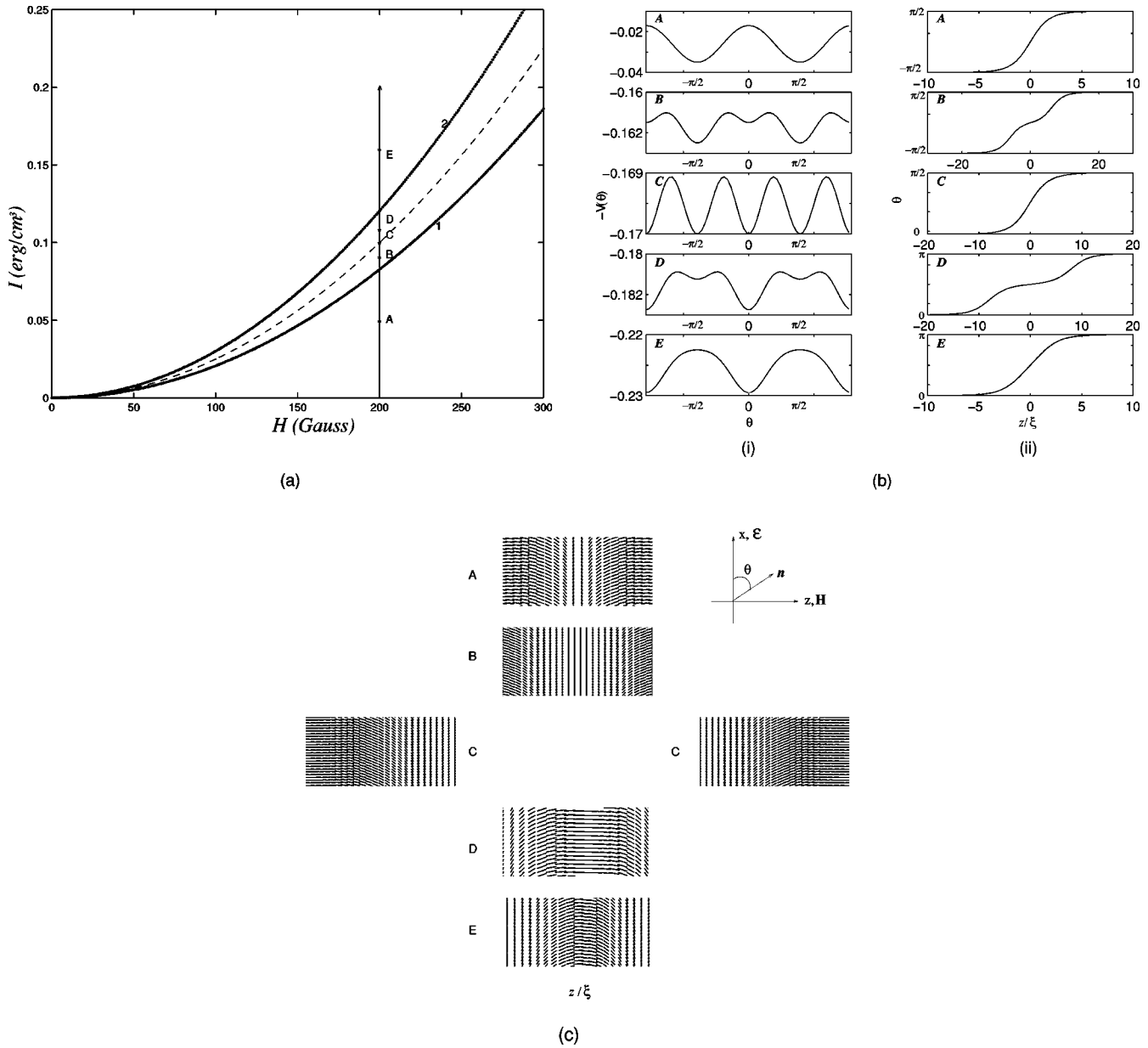

FIG. 2. (a) Phase diagram for the uniform state as well as the kink state in a nematic. The dashed curve is a line of first order transition The dotted lines 1 and 2 are stability lines. Here I is the measure of intensity. $\epsilon_{\parallel}=2.89$, $\epsilon_{\perp}=2.25$, and $K=10^{-6}$ dyn. (b) (i) Effective potential V as a function of θ. (ii) Kink solutions. Here θ is in rad and $\xi^2=K/\chi_a H^2$ is the coherence length. (c) Director configuration of the kinks in the regions A,B,C,D, and E of the phase diagram (a).

where $k_0=\omega/c$, A is the amplitude of the light wave, and $\theta\equiv\theta(z)$ is the angle between the director $\mathbf{n}$ and the $\boldsymbol{\mathcal{E}}$ vector. Then from Eqs. (3), (5), and (6), the optical field free energy density becomes

$$\mathcal{F}_o=-I\frac{(\epsilon_{\parallel}\epsilon_{\perp})^{1/2}}{(\epsilon_{\perp}+\epsilon_a\sin^2\theta)^{1/2}}, \tag{7}$$

where $I[=(|A|^2/8\pi c)(\epsilon_{\parallel}\epsilon_{\perp})^{1/2}]$ is a measure of the intensity of light. We note that in the limit of small dielectric anisotropy or for small director distortions, $\mathcal{F}_o$ goes over to the familiar expression for the field contribution to free energy density in static electric fields.

It must be remarked that in any other geometry either the polarization of the light wave may change and or the phase also may vary across the wave front as it propagates through the kink structure. In the case of a twist wall in the geometrical optics approximation, applicable to cases with director distortions along the direction of light propagation, the direction of light propagation is along the helix axis. In this approximation the director distortions are on a length scale very large compared to the wavelength of the light. Then for the twist wall this leads to the Maugin limit or adiabatic limit. In this limit the base states are linearly polarized parallel or perpendicular to the local director. Hence if the incident light is initially polarized parallel to the director, then it always remains parallel to the local director. This does not result in any change in the director configuration, as it does not lead to any optical torque on the director. Only at low magnetic fields is this approximation valid and the wall

structure unaffected. At higher fields this approximation breaks down since the wall thickness may become comparable to or less than the wavelength of the light. In such cases we find that there could be reflection and/or diffraction of light by the soliton; also, the polarization state of the laser wave is not preserved as it propagates through the soliton. Further, if the incident light is initially perpendicular to the director, then the kink structure remains unaffected up to a threshold intensity of the laser. Beyond this threshold intensity the director configuration in the kink structure is affected. These situations lead to complex director configurations, and a complete solution will be an involved numerical exercise when finding the solution of Maxwell's equations and the equations of elastic equilibrium. Such situations are not considered in this investigation.

We have confined our studies to planar distortions involving splay and bend only. The splay-rich and bend-rich kinks involve both types of distortions, and no qualitative changes are found if elastic anisotropy is included, i.e., the splay elastic constant is not equal to the bend elastic constant. In fact we observe that elastic anisotropy leads only to an increase or decrease in the thickness of the wall depending on the sign of the anisotropy. Hence to extract the salient features we have adopted a one constant approximation.

Before proceeding further we remark on the influence of the boundaries. Two possible geometries are (1) boundaries are parallel to the wall, and (2) boundaries are perpendicular to the wall. In the case of boundaries parallel to the wall, the director, which is assumed to be anchored at the boundaries, will influence the distortion in the bulk. Here the exercise of solving Maxwell's equations and equations of elastic equilibrium become boundary value problems which add to the computational complexity. In the case of boundaries perpendicular to the wall, we obtain a half strength defect at each boundary. This configuration affects the phase across a plane wave front of light incident on the wall, and hence does not conform to the geometrical optics approximation. Similar arguments are valid for Brochard-Leger walls, briefly described in Sec. I. This also leads to the reflection and/or diffraction of the laser wave, and hence we do not consider it in this study.

It is important to point out the salient features peculiar to the nonlinear optical reorientation effects as compared to reorientational effects in static electric fields. In the optical case the Maxwell's equation $\nabla\cdot\boldsymbol{\mathcal{D}}=0$ leads, in the plane wave approximation, to $\mathbf{k}\cdot\boldsymbol{\mathcal{D}}=0$, where $\mathbf{k}$ is the direction of light propagation. In view of the fact that the propagation is along z, the variations in the field are also along z. This implies that the component $\boldsymbol{\mathcal{D}}_z$ vanishes identically. Since $\boldsymbol{\mathcal{D}}_z=\Sigma_i\epsilon_{zi}\boldsymbol{\mathcal{E}}_i$ and $\boldsymbol{\mathcal{E}}_y=0$, we obtain $\boldsymbol{\mathcal{E}}_z=-(\epsilon_{zx}/\epsilon_{zz})\boldsymbol{\mathcal{E}}_x$. Equation (6) has been obtained from Eq. (5) using this relation. Further, both $\boldsymbol{\mathcal{E}}_z$ and $\boldsymbol{\mathcal{E}}_x$ are complex functions of z. On the other hand, in the case of the static field we have the two Maxwell's equations $\nabla\times\mathbf{E}=\mathbf{0}$ and $\nabla\cdot\mathbf{D}=\mathbf{0}$. The first of these equations leads to the relation $\partial E_x/\partial z=0$, and hence E_x is a constant. The second equation, with appropriate boundary conditions, again implies $D_z=0$ thus leading to the same relation between E_x and E_z. The dependence of E_z on z coordinate is not through E_x but only due to spatial variations in the dielectric tensor components ϵ_{zx} and ϵ_{zz}. Hence instead of Eqs. (5) and (6), in the case of static fields we obtain $E_x=\text{const}$ and $E_z=\epsilon_a\sin\theta\cos\theta E_x/(\epsilon_\perp+\epsilon_a\sin^2\theta)$.

III. KINK STATES

A. Kinks in an optical field

We first study kinks permitted in an optical field. The relevant geometry is that shown in Fig. 1(a). The free energy density for planar distortions is

$$\mathcal{F}=\frac{K}{2}\left(\frac{\partial\theta}{\partial z}\right)^2-\frac{I\epsilon_\parallel^{1/2}}{(1+\mu\sin^2\theta)^{1/2}}.$$

Here $\mu=\epsilon_a/\epsilon_\perp$. The kink state has only splay-bend distortions in the director. Minimization of the total free energy leads to

$$K\frac{\partial^2\theta}{\partial z^2}=\frac{I\epsilon_\parallel^{1/2}\mu\sin\theta\cos\theta}{(1+\mu\sin^2\theta)^{3/2}}.$$

The equation of equilibrium in an optical field is no longer the familiar sine-Gordon equation that we obtain for static magnetic fields. Numerically we find, using the Runge-Kutta-Fehlberg method, solutions to the above equilibrium equation. These kinks are found to be essentially similar to the kinks permitted in static magnetic fields.

B. Kinks in magnetic and optical fields

1. Nematic

We now consider the effect of the electrical field $\boldsymbol{\mathcal{E}}$ of the light wave on kinks that are already present in the presence of an external magnetic field. The different geometries which could be studied include the electric field of the light wave $\boldsymbol{\mathcal{E}}$ being either parallel or perpendicular to the static magnetic field $\mathbf{H}$ with ϵ_a and χ_a being positive or negative.

We discuss only one geometry shown in Fig. 1(b), where $\boldsymbol{\mathcal{E}}$ is perpendicular to $\mathbf{H}$ and both ϵ_a and χ_a are positive. The corresponding equation of equilibrium is

$$K\frac{\partial^2\theta}{\partial z^2}=\frac{I\epsilon_\parallel^{1/2}\mu\sin\theta\cos\theta}{(1+\mu\sin^2\theta)^{3/2}}-\chi_aH^2\sin\theta\cos\theta. \qquad (8)$$

It is clear from Eq. (8) that the torque acting on the director due to the static magnetic field $\mathbf{H}$ opposes that due to the electric field $\boldsymbol{\mathcal{E}}$ of the light wave.

We first work out the different uniform states permitted by Eq. (8). In the uniform state the director $\mathbf{n}$ can be either parallel ($\theta=0$) or perpendicular ($\theta=\pi/2$) to the electric field $\boldsymbol{\mathcal{E}}$. As to which is allowed is obtained by appealing to the free energy. There can be a switch over from one uniform state to the other as either I or $\mathbf{H}$ is changed. The phase diagram so obtained is shown in Fig. 2(a). The dashed line in the phase diagram is a line of coexistence of the two states with $\theta=0$ and $\pi/2$. The dotted lines 1 and 2 are lines of stability across which a particular orientation of the director goes from an unstable state to a metastable state, and *vice versa*.

Now we take up kink states that can exist in the same geometry. We solve Eq. (8) to obtain the permitted kink

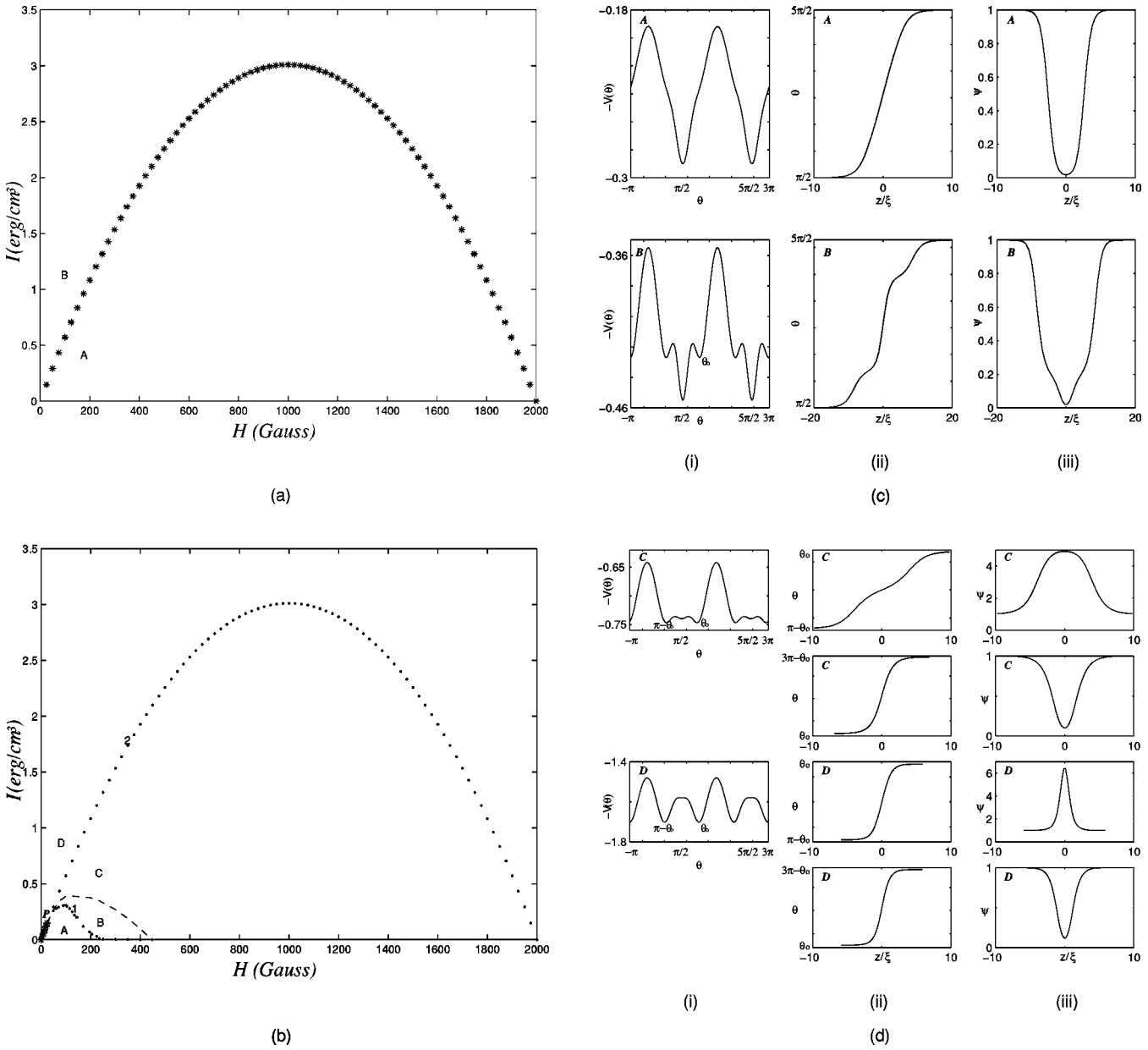

FIG. 3. Phase diagram for the uniform state of a ferronematic with $\boldsymbol{\mathcal{E}}$ perpendicular to **H**, $\epsilon_a>0$, $\chi_a<0$, and **M** parallel to **H**. The starred curve is a line of second order transition. In all our calculations in a ferronematic we have used the parameters $m=2$ G, $\rho=mv/k_BT=0.02$ G^{-1}, $\bar{f}=10^{-3}$, and $\chi_a=10^{-6}$ cgs. (b) Phase diagram for kink states in the geometry considered in (a). The starred curve represents a second order transition. The dashed curve is a line of first order transition. The dotted lines are stability lines. *P* is a tricritical point. (c) (i) Effective potential *V* as a function of θ. (ii) Kink solutions and (iii) grain profiles in regions *A* and *B* of the phase diagram (b). $\psi=f/\bar{f}$. (d) (i) Effective potential *V* as a function of θ. (ii) Kink solutions and (iii) grain profiles in regions *C* and *D* of the phase diagram (b).

states. Interestingly, we find that the phase diagram for transition between different permitted kink states is the same as that for uniform states. In this calculation we have utilized the particle analogy [5]. We define an effective potential $V(\theta)$ as

$$V(\theta)=\frac{I\epsilon_{\parallel}^{1/2}}{(1+\mu\sin^2\theta)^{1/2}}+\frac{\chi_a}{2}H^2\sin^2\theta.$$

Then Eq. (8) can be written as

$$K\frac{\partial^2\theta}{\partial z^2}=-\frac{\partial V}{\partial\theta}.$$

The uniform states are given by the minima of $-V(\theta)$. The potential as a function of θ and the permitted kink solutions in regions A,B,C,D, and E of the phase diagram are shown in Figs. 2(b) and 2(c), respectively. In Fig. 2(d) we show the director profiles of the kink states permitted in these regions. The flat region in a kink profile corresponds to a local minima in $-V$, or equivalently to a metastable state. As we go from *A* to *E*, the laser intensity *I* or consequently the electric field $\boldsymbol{\mathcal{E}}$ increases in magnitude. We obtain a splay-rich kink in region *A*, while we end up with a bend-rich kink in region *E*. There is a first order transition between these two kink states. On the dashed line, two new kink states connecting $-\pi/2$ to 0 and 0 to $\pi/2$ become permitted solutions. This is unlike in a nematic in external static fields,

TABLE II. The various stable and metastable states of the uniform and kink states in the different regions of their phase diagrams shown in Figs.3(a) and 3(b), respectively.

Region	Uniform state				Kink state		
	Stable states		Metastable states		Topological charge	Split occurs at	
A	$\pi/2$	$5\pi/2$			2π		
B	$\pi/2$	$5\pi/2$	θ_0	3π-θ_0	(i) 2π (ii) 3π-$2\theta_0$	θ_0	3π-θ_0
C	π-θ_0	θ_0	$\pi/2$		(i) $2\theta_0$-π (ii) 3π-$2\theta_0$	$\pi/2$	
D	π-θ_0	θ_0			(i) $2\theta_0$-π (ii) 3π-$2\theta_0$		

where the kink connects only 0 (or $-\pi/2$) and π (or $\pi/2$) states. Hence the scenario is like this: a $(-\pi/2)\rightarrow\pi/2$ splay-rich kink becomes unstable along the dotted line 1, and splits into a bound pair of $-\pi/2\rightarrow 0$ and $0\rightarrow\pi/2$ kinks linked by a $\theta=0$ uniform state. As I increases further, the separation increases, and it diverges to infinity as the dashed line is approached. On the other side of the dashed line the permitted kink solution is a bound kink pair of $0\rightarrow\pi/2$ and $\pi/2\rightarrow\pi$. Finally these two merge after the dotted line 2 is crossed, to result in a $0\rightarrow\pi$ bend-rich kink. The results are summarized in Table I. This depicts only one set of permitted solutions and not their symmetry related ones. Here the topological charge is the total change in the director orientation across the kink. The same results are obtained for the case of $\boldsymbol{\mathcal{E}}$ parallel to **H**, but with ϵ_a positive and χ_a negative.

2. Ferronematic

Due to an increase in the number of independent parameters in ferronematics, we have many more possibilities. Here **M** can be either parallel or antiparallel to **H** with ϵ_a and χ_a positive or negative. For the purposes of our discussion here we treat only the following two cases since these exhibit some new and interesting features:

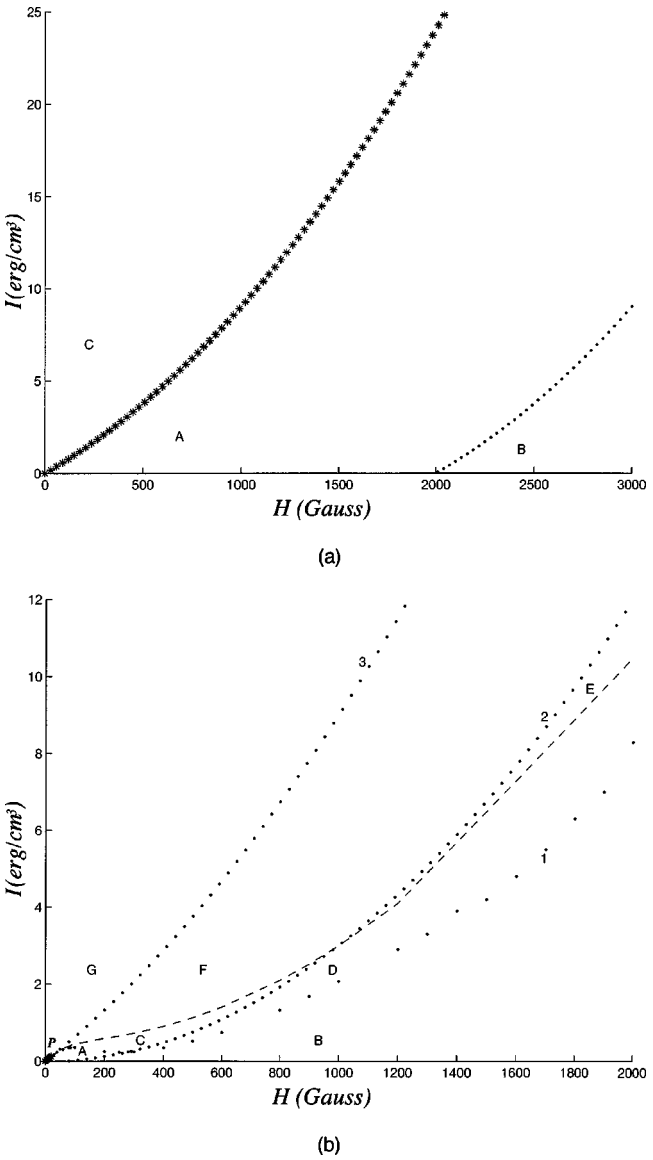

FIG. 4. Phase diagram for the uniform state of a ferronematic with $\boldsymbol{\mathcal{E}}$ perpendicular to **H**, $\epsilon_a>0$, $\chi_a>0$, and **M** parallel to **H**. The starred line represents a second order transition. The dotted line is a line of stability. (b) Phase diagram for kink states in the geometry considered in (a). Starred and dashed curves are lines of second and first orders, respectively. Dotted lines 1, 2, and 3 are stability lines. *P* is the tricritical point.

Case I $\Rightarrow\boldsymbol{\mathcal{E}}$ perpendicular to **H**, $\epsilon_a>0$, $\chi_a<0$ and **M** parallel to **H**,

Case II $\Rightarrow\boldsymbol{\mathcal{E}}$ perpendicular to **H**, $\epsilon_a>0$, $\chi_a>0$ and **M** parallel to **H**.

The other cases are similar to one or the other of these two cases. We discuss the first case in detail.

(a) Case I

Phase diagram for the uniform state. The geometry for this case is depicted in Fig. 1(b). The free energy density of a ferronematic in a static magnetic field in the presence of a laser field is obtained by adding Eqs. (1), (2), and (7), i.e.,

$$\mathcal{F}=\frac{K}{2}\left(\frac{\partial\theta}{\partial z}\right)^2-\frac{I\epsilon_{\parallel}^{1/2}}{(1+\mu\sin^2\theta)^{1/2}}+\frac{|\chi_a|}{2}H^2\sin^2\theta-mfH\sin\theta+\frac{fk_BT\ln f}{v},\tag{9}$$

where m is the average magnetization of an individual grain.

TABLE III. The various stable and metastable states of the uniform and kink states in the different regions of their phase diagrams shown in Figs. 4(a) and 4(b), respectively.

Region	Uniform state					Kink state			
	Stable states		Metastable states			Topological charge	Split occurs at		
A	$\pi/2$	$5\pi/2$				2π			
B	$\pi/2$	$5\pi/2$		$3\pi/2$		2π		$3\pi/2$	
C	$\pi/2$	$5\pi/2$		θ_0	3π-θ_0	(i) 2π (ii) 3π-$2\theta_0$	θ_0	3π-θ_0	
D	$\pi/2$	$5\pi/2$	θ_0	$3\pi/2$	3π-θ_0	(i) 2π (ii) 3π-$2\theta_0$	θ_0	$3\pi/2$ $3\pi/2$	3π-θ_0
E	π-θ_0	θ_0	$\pi/2$	$3\pi/2$		(i) $2\theta_0$-π (ii) 3π-$2\theta_0$	$\pi/2$	$3\pi/2$	
F	π-θ_0	θ_0	$\pi/2$			(i) $2\theta_0$-π (ii) 3π-$2\theta_0$	$\pi/2$		
G	π-θ_0	θ_0				(i) $2\theta_0$-π (ii) 3π-$2\theta_0$			

In the uniform state of a ferronematic there is no grain segregation, and therefore f is a constant. Hence the last term in the free energy is a constant. The uniform states are obtained from

$$\frac{I\epsilon_{\parallel}^{1/2}\mu \sin\theta\cos\theta}{(1+\mu\sin^2\theta)^{3/2}}+|\chi_a|H^2\sin\theta\cos\theta-mfH\cos\theta=0. \tag{10}$$

The permitted uniform states are (i) **n** along the magnetic field ($\theta=\pi/2$ or $5\pi/2$) and (ii) **n** at an angle to the field ($\theta=\theta_0$ or $\pi-\theta_0$). The phase diagram for the transition between these permitted uniform states is depicted in Fig. 3(a). The transition from one uniform state to another in this case is of second order. In region *A* we have $\theta=\pi/2$ (or $5\pi/2$), and in the region *B* $\theta=\theta_0$ (or $\pi-\theta_0$). One interesting feature of this case should be stressed here. At a constant optical intensity below a threshold value, when the magnetic field is continuously increased the system undergoes a transition from a uniform state with $\theta=\theta_0$ (or $\pi-\theta_0$) to another uniform state with $\theta=\pi/2$ (or $5\pi/2$) and returns back to the initial uniform state, i.e., $\theta=\theta_0$ (or $\pi-\theta_0$). Thus the system exhibits a reentrant phenomenon.

Phase diagram for the kink states. In the case of kinks, different parts of the kink are at different orientations with respect to **H**. This causes the grains to migrate to regions of lower energy. Hence the grain concentration and thus f are not constants. We then have to minimize the total free energy both with respect to f and θ to find the equilibrium director configuration.

Minimization with respect to f leads to

$$f=C\exp(\rho H\sin\theta-1), \tag{11}$$

where C is a constant of integration and $\rho=$mv/kBT.

Since a kink connects two uniform states, the orientation θ_∞ of the uniform state at $z=\pm\infty$ can be obtained from a minimization of the total free energy by neglecting the ''grain segregation.'' With the boundary condition $f=\bar{f}$ at $z=\pm\infty$ and $\theta=\theta_\infty=\theta_0$ (or $\pi/2$), Eq. (11) becomes

$$f=\bar{f}\exp[\rho H(\sin\theta-\sin\theta_\infty)]. \tag{12}$$

Minimization with respect to θ yields

$$K\frac{\partial^2\theta}{\partial z^2}=\frac{I\epsilon_{\parallel}^{1/2}\mu\sin\theta\cos\theta}{(1+\mu\sin^2\theta)^{3/2}}+|\chi_a|H^2\sin\theta\cos\theta-m\bar{f}H\exp[\rho H(\sin\theta-\sin\theta_\infty)]\cos\theta. \tag{13}$$

We solve this equation numerically to obtain kink solutions. The kink structures will be sensitive to I and **H**. The kink states permitted in this case are $\pi/2\rightarrow5\pi/2$, $(\pi-\theta_0)\rightarrow\theta_0$ and $\theta_0\rightarrow(3\pi-\theta_0)$. The resulting phase diagram for the kink state is shown in Fig. 3(b). Up to a certain magnetic field, the order of transition between a $\pi/2\rightarrow5\pi/2$ kink and a $(\pi-\theta_0)\rightarrow\theta_0$ or $\theta_0\rightarrow(3\pi-\theta_0)$ kink is second order. Beyond this field strength this transition becomes first order. Thus there is a *tricritical* point in the phase diagram. The tricritical point can be fixed by appealing to the grain segregation term. The condition is then $\rho|\mathbf{H}|=1$. The dotted lines 1 and 2 are stability lines.

Again utilizing the particle analogy, we define an effective potential

$$V(\theta)=\frac{I\epsilon_{\parallel}^{1/2}}{(1+\mu\sin^2\theta)^{1/2}}-\frac{|\chi_a|}{2}H^2\sin^2\theta+m\bar{f}H\times\exp[\rho H(\sin\theta-\sin\theta_\infty)].$$

Figures 3(c), 3(d), and 3(e), respectively, show the potential, the kink states, and the grain profile in regions A,B,C, and D of the phase diagram. In addition, the phase diagram shows reentrance of a kink state below a certain threshold value of the light intensity. We have summarized the salient features of the uniform and kink states in Table II. We have not explicitly depicted the symmetry related solutions.

(b) Case II

The geometry of the problem for this case is shown in Fig. 1(b). In this case the phase diagram for the uniform state and the kink state are shown in Figs. 4(a) and 4(b), respectively. The starred line in Fig. 4(a) is a line of second order phase transition, and the dotted line is a line of stability. The permitted kink states are $\pi/2 \rightarrow 5\pi/2$, $(\pi-\theta_0) \rightarrow \theta_0$ and $\theta_0 \rightarrow (3\pi-\theta_0)$. The phase diagram is richer here than in the previous cases. Here all the interesting features which we obtained in the previous cases are present in this one system. A small region in the phase diagram shown in Fig. 4(b) shows reentrant behavior, and there are regions where there are new stable states. Interestingly, reentrant behavior is not seen in the phase diagram for the uniform states. On the dashed line in Fig. 4(b) we find a transformation of a $\pi/2 \rightarrow 5\pi/2$ kink into a pair of kinks *viz.* $(\pi-\theta_0) \rightarrow \theta_0$ and $\theta_0 \rightarrow (3\pi-\theta_0)$. This transformation is second order at low I and **H** and first order at higher values of I and **H** implying the existence of a *tricritical* point on this line. The dotted lines 1, 2, and 3 are stability lines. Table III gives the essential features of the uniform and permitted kink states in the different regions of the phase diagram. Here too we can generate symmetry related solutions from the ones given in the table.

IV. CONCLUSIONS

We have worked out the phase diagram of transitions for the uniform and kink states of nematics and ferronematics due to nonlinear optical interactions with a laser field. We find a first order transition between the permitted uniform states in nematics. This allows the existence of new instabilities and kink states. Both uniform and kink states have the same phase diagram. In the case of ferronematics the transition between the permitted uniform states is of second order, exibiting in addition the phenomenon of reentrance. In the case of transformations between the kink states the transition could be of first or second order with an associated *tricritical* point. Here also we find a reentrance phenomenon. Further, due to grain seggregation the phase diagrams of the uniform and the kink states are entirely different.

ACKNOWLEDGMENTS

Our thanks are due to K.A. Suresh and Sreejith Sukumaran for helpful comments.

[1] I.C. Khoo and S.T. Wu, *Optics and Non-linear Optics of Liquid Crystals* (World Scientific, Singapore, 1993).
[2] F. Simoni, *Nonlinear Optical Properties of Liquid Crystals and Polymer Dispersed Liquid Crystals* (World Scientific, Singapore, 1997).
[3] N.V. Tabiryan, A.V. Sukhov, and B.Ya. Zel'dovich, Mol. Cryst. Liq. Cryst. **136**, 1 (1986).
[4] F. Simoni, Liq. Cryst. **24**, 83 (1998).
[5] *Solitons in Liquid Crystals*, edited by L. Lam and J. Prost (Springer-Verlag, Berlin, 1991).
[6] W. Helfrich, Phys. Rev. Lett. **21**, 1518 (1968).
[7] P.G. de Gennes, Solid State Commun. **6**, 163 (1968).
[8] R.B. Meyer, Appl. Phys. Lett. **12**, 281 (1968).
[9] M. Yamashita, H. Kimura, and H. Nakamo, Mol. Cryst. Liq. Cryst. **68**, 79 (1981).
[10] P.G. de Gennes and J. Prost, *The Physics of Liquid Crystals* (Oxford Science Publications, Oxford, 1993).
[11] F. Brochard and P.G. de Gennes, J. Phys. (France) **31**, 691 (1970).
[12] H.L. Ong, Phys. Rev. A **28**, 2933 (1982).